remote sensing

MDPI

Article

An Integration of Deep Learning and Transfer Learning for Earthquake-Risk Assessment in the Eurasian Region

Ratiranjan Jena [1], Abdallah Shanableh [1,2], Rami Al-Ruzouq [1,2], Biswajeet Pradhan [3,4], Mohamed Barakat A. Gibril [1], Omid Ghorbanzadeh [5,6,*], Clement Atzberger [6], Mohamad Ali Khalil [1], Himanshu Mittal [7] and Pedram Ghamisi [5,8]

1 GIS & Remote Sensing Center, Research Institute of Sciences and Engineering, University of Sharjah, Sharjah 27272, United Arab Emirates; rjena@sharjah.ac.ae (R.J.)
2 Civil and Environmental Engineering Department, University of Sharjah, Sharjah 27272, United Arab Emirates
3 Centre for Advanced Modelling and Geospatial Information Systems (CAMGIS), School of Civil and Environmental Engineering, Faculty of Engineering and Information Technology, University of Technology Sydney, Ultimo, NSW 2007, Australia
4 Earth Observation Centre, Institute of Climate Change, Universiti Kebangsaan Malaysia (UKM), Bangi 43600, Selangor, Malaysia
5 Institute of Advanced Research in Artificial Intelligence (IARAI), Landstraßer Hauptstraße 5, 1030 Vienna, Austria
6 Institute of Geomatics, University of Natural Resources and Life Sciences, Vienna, Peter-Jordan Strasse 82, 1190 Vienna, Austria
7 National Center for Seismology, Ministry of Earth Sciences, Government of India, New Delhi 110003, India
8 Helmholtz-Zentrum Dresden-Rossendorf, Helmholtz Institute Freiberg for Resource Technology, MachineLearning Group, Chemnitzer Street 40, 09599 Freiberg, Germany
* Correspondence: omid.ghorbanzadeh@boku.ac.at

Abstract: The problem of estimating earthquake risk is one of the primary themes for researchers and investigators in the field of geosciences. The combined assessment of spatial probability and the determination of earthquake risk at large scales is challenging. To the best of the authors' knowledge, there no updated earthquake-hazard-and-risk assessments for the Eurasia region have been published since 1999. Considering that Eurasia is characterized by a seismically active Alpine–Himalayan fault zone and the Pacific Ring of Fire, which are frequently affected by devastating events, a continental-scale risk assessment for Eurasia is necessary to check the global applicability of developed methods and to update the earthquake-hazard, -vulnerability, and -risk maps. The current study proposes an integrated deep-transfer-learning approach called the gated recurrent unit–simple recurrent unit (GRU–SRU) to estimate earthquake risk in Eurasia. In this regard, the GRU model estimates the spatial probability, while the SRU model evaluates the vulnerability. To this end, spatial probability assessment (SPA), and earthquake-vulnerability assessment (EVA) results were integrated to generate risk A, while the earthquake-hazard assessment (EHA) and EVA were considered to generate risk B. This research concludes that in the case of earthquake-risk assessment (ERA), the results obtained for Risk B were better than those for risk A. Using this approach, we also evaluated the stability of the factors and interpreted the interaction values to form a spatial prediction. The accuracy of our proposed integrated approach was examined by means of a comparison between the obtained deep learning (DL)-based results and the maps generated by the Global Earthquake Model (GEM). The accuracy of the SPA was 93.17%, while that of the EVA was 89.33%.

Keywords: earthquake risk; hazard assessment; vulnerability mapping; artificial intelligence (AI); transfer learning; Eurasia

Citation: Jena, R.; Shanableh, A.; Al-Ruzouq, R.; Pradhan, B.; Gibril, M.B.A.; Ghorbanzadeh, O.; Atzberger, C.; Khalil, M.A.; Mittal, H.; Ghamisi, P. An Integration of Deep Learning and Transfer Learning for Earthquake-Risk Assessment in the Eurasian Region. *Remote Sens.* **2023**, *15*, 3759. https://doi.org/10.3390/rs15153759

Academic Editor: Benoit Vozel

Received: 25 May 2023
Revised: 22 July 2023
Accepted: 25 July 2023
Published: 28 July 2023

1. Introduction

Earthquakes are the most catastrophic phenomena to seriously threaten urban areas. Recently, the importance of earthquake-risk analysis has increased, particularly the analysis of the safety of the design of structures associated with nuclear power plants and chemical industries [1]. Consequently, several studies have attempted to provide different techniques to assess and manage earthquake risk around the world. For instance, the protection of nuclear power plants against earthquake risk was evaluated in several studies [2–5]. Moreover, geographical information systems (GIS) and artificial intelligence (AI) techniques were adopted to identify suitable locations for nuclear plants by estimating earthquake risk [6,7]. Earthquake-risk estimation is greatly dependent on the integrated capability of seismological, geological, and geotechnical effects [8]. Therefore, the problem of earthquake risk must be dealt with by researchers and scientists from multiple disciplinary fields.

Pourghasemi et al. [9] conducted a study on multi-hazard-probability assessment in Iran. In their work, an earthquake-probability map, which mostly covered the Zagros–Bitlis thrust fault, was designed, with an accuracy of more than 80%. Durlević et al. [10] generated a multi-hazard-probability map for southern Serbia. They found high spatial probability in the resulting multi-hazard map. Tang et al. [11] evaluated seismic spatial and temporal distribution quantitatively based on a single fractal model. Their results showed that the time interval of the seismic activity was shortened, and the fractal dimension of the Eurasian seismic belt tended to grow with time. In the Eurasia seismic belt, Zheng et al. [12] determined the temporal and spatial distribution of earthquakes. According to their results, the seismic energy of the earthquake fault zone has both a relatively quiet and an active stage. The study conducted by Shebalin et al. [13] examined the unified seismotectonic zonation in Northern Eurasia. They estimated the possible events that feature the maximum magnitude, and the recurrence period was determined using seismological and active fault parameters. Genmo et al. [14] performed a study on the space–time distribution of large earthquakes in the Indian–Eurasian plate-collision zone. The study described the possibility of greater events in the next few decades, along the eastern part of the Himalayas and in the central parts of the Asian continent.

A review of the seismic hazards estimated in the former USSR since 1930 was conducted by Ulomov et al. [15], and five seismic-hazard maps were produced for northern Eurasia. Ulomov [16,17] and the Global Seismic Hazard Assessment Program (GSHAP)'s regional center conducted this study on seismic-hazard assessment in northern Eurasia using a deterministic–probabilistic approach. The study showed the expected MSK intensity (VII) and its transformation into peak ground acceleration (PGA) with a 10% exceedance rate over 50 years. Regional and country-scale studies are recorded in the literature on (EHA) in the Himalayan region [18,19]. Strakhov et al. [20] developed general seismic-zoning maps of northern Eurasia, generated seismic-effect models and earthquake-source zones, and conducted seismic-hazard assessments. Lapajne [21] incorporated the macro-seismic intensity to estimate seismic risk. For a given distribution of seismic hazard, temporal changes and regional differences must be properly incorporated for risk estimation. Using a probabilistic approach based on seismographic data, Shapira [22] evaluated the earthquake risk at the Afro–Eurasian junction. In order to evaluate the validity of the proposed approach, a comparison between the obtained results and the historical seismicity was made. Gupta and Srivastav [23] conducted an earthquake-risk assessment in the Himalayan region and its adjoining areas. Based on their findings, a realistic estimation of earthquake recurrence, the construction of geodynamic models, and the determination of source parameters are essential for the estimation of risk. An assessment of earthquake vulnerability for energy security in the Eurasian Economic Union was carried out by Iakubovskii et al. [24]. This study applied a mathematical model to estimate the reliability of the electricity-supply system under the threat of earthquakes. It determined the critical interconnection lines that are vulnerable to earthquake hazards. Jackson [25] evaluated the effect of earthquake vulnerability on the growth of villages into megacities. This study mentioned that extreme catastrophes are infrequent because of the low exposure of modern cities. Several earthquake-vulnerability

studies can be found in the literature on buildings [26], transportation networks [27], urban areas [28], and engineering structures [29].

The above-mentioned studies suggest that earthquakes associated with the Alpine–Himalayan belt, the Pacific Ring of Fire, and local faults in Eurasia have caused massive destruction. Few EHA studies on a continent scale have been conducted in Eurasia. As a research gap, machine learning and deep learning (DL) models have also not been implemented in Eurasia. Furthermore, no integrated deep-transfer-learning models to estimate earthquake risk on a continent scale can be found in the literature. Limited research on regional-to-national-scale earthquake-risk assessment can be found in the literature using GIS and AI techniques [9,10]. This study fills this research gap. As a novelty in this study, the risk was assessed by following two definitions of natural hazards, according to which the probability and vulnerability were estimated using the deep-transfer-learning model. Two maps, named Risk A and Risk B, were developed and compared, followed by the spatial probability, hazard, and vulnerability. Earthquake-risk assessment is generally associated with the challenges of modeling complexities, data limitations, and accuracy [9]. The purpose of this article is to address the challenges associated with the inaccessibility of data, the integration of spatial information, and the combination of different methodological concepts, as well as addressing the secondary effects. The largest continental area on Earth is the Eurasian continent, which is exposed to high levels of earthquake hazard due to large-magnitude events originating in the Alpine–Himalayan belt [17]. In this work, we quantify the present-day earthquake risk using an integrated deep-transfer-learning technique. Our main concern is to develop an approach to the design of an earthquake-spatial-probability map (SPM), hazard estimation using Medvedev–Sponheuer–Karnik scale (MSK) intensity, a vulnerability assessment, and a risk evaluation. The main contribution of this work lies in the application of an integrated deep-learning model for a continent-scale study area using a geospatial approach to update the earthquake risk in Eurasia. Another contribution of the current study leverages the hidden interaction of factors and their relative importance. The main objectives are: (i) to estimate the SPA using the GRU model and to evaluate the EHA using the MSK intensities in the study area; and (ii) to derive the vulnerability using the population density, building density, public education, gross development products, industries, and income-level data by implementing the SRU model. In this context, (iii) to depict the ERA in Eurasia, the integration of hazard and vulnerability was conducted. This study constitutes a first step towards supporting decision makers in understanding and taking proper actions to reduce potential losses in Eurasia.

2. Seismotectonic of the Study Area

Physiographically, Eurasia is the single largest continental area on Earth, characterized by a land surface of 55,000,000 km^2 (21,000,000 sq. mi) [30]. There is no clear physical divisional boundary between Europe and Asia; this boundary is a fully social construct, making Eurasia the largest continent on Earth. The total population of Eurasia is approximately 5,360,351,985, with a density of 93/km^2 (240/sq. mi) (Population of Europe (2019)—Worldometers; Population of Asia (2019)—Worldometers) [30,31]. The geology and major events and fault types in Eurasia are shown in Figure 1.

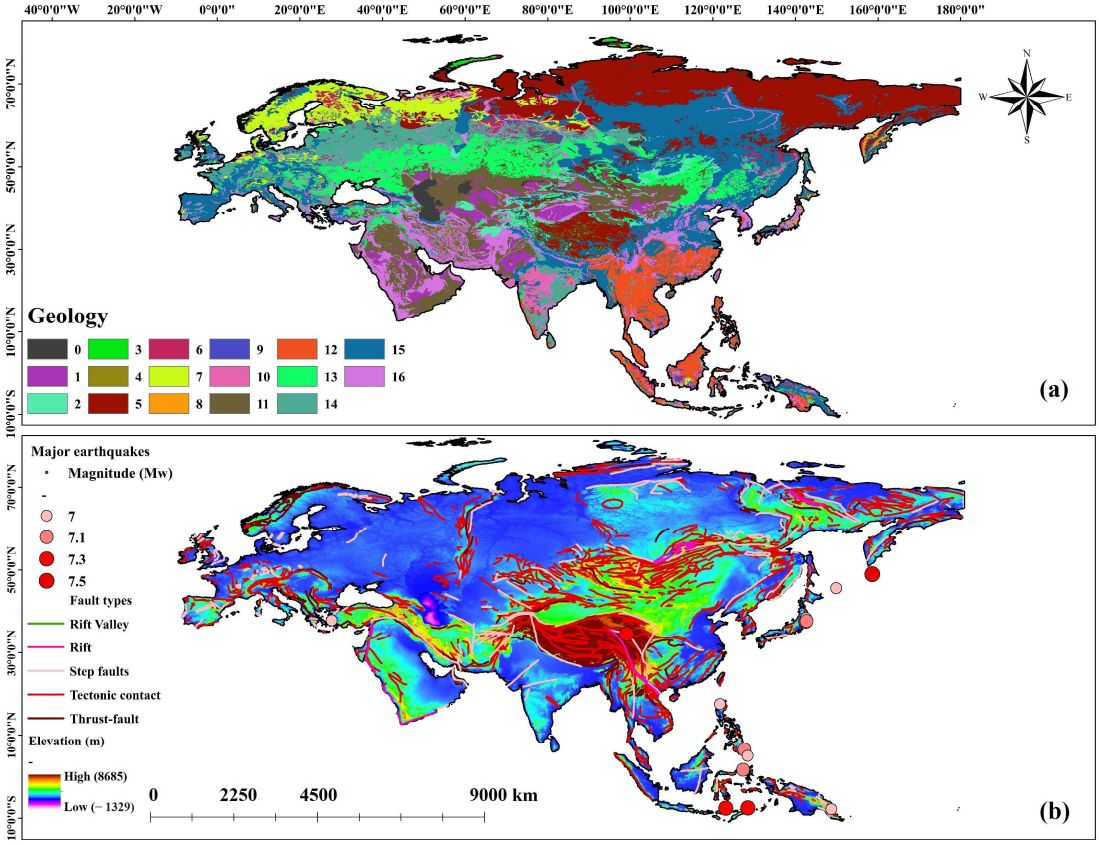

Figure 1. Study-area map of Eurasia. (**a**) Geology: 0 water), 1 (shifting sands), 2 (rocky land), 3 (ice/glacier), 4 (salt), 5 (gelisols), 6 (histosols), 7 (spodosols), 8 (andisols), 9 (oxisols), 10 (vertisols), 11 (aridisols), 12 (ultisols), 13 (mollisols), 14 (alfisols), 15 (inceptisols), 16 (entisols). (**b**) Major events and faults in Eurasia.

Seismic zones are the specific regions of the Earth for which a common seismicity rate is assumed to calculate probabilistic ground motions. The major seismic-zone characteristics are magnitude–frequency relationships, strain release, and fault-plane solutions. The Eurasian continent is composed of 93 countries [32]. Central Eurasia is one of the most significant areas of seismic activity, and it is governed by intense interactions between tectonic plates and continental blocks, such as northern Eurasia, Arabian plate, African plate, Indian sub-continent, eastern China, North America, Pacific plate, etc. [33]. The heterogeneity of the tectonic structure is at different scales (crustal scale to regional scale); therefore, it is necessary to investigate the static and dynamic characteristics of tectonic objects. Eurasia is characterized by very low, diffuse (Russian and Siberian land), and severe seismicity in the orogenic belts (Alpine–Himalayan Belt) [17,20]. The most geo-dynamically active zone, named the Kuril–Kamchatka subduction zone, is a region of high seismicity, with earthquakes focus, at depths of 600 km and more. The thickness of the platform's crust is 40 $\pm$ 5 km, while the orogenic belts reach 60 km [34]. Other subduction zones, such as the Carpathians and Pamir Hindukush zones, generate intermediate-focus earthquakes (depth range from 150 km to 300 km). The relict-deformation zone and intracontinental seismic regions [15,16] are subject to deformation processes, resulting in high seismicity. Therefore, each seismic zone is considered as a feature that controls the seismicity of the region.

The hierarchical structure of intraplate earthquakes can be determined by historical geological processes that are controlled by Quaternary and recent tectonic activities [17]. The size of the active-fault-plane area controls the earthquake-magnitude limit, whereas the number and rank of faults and the fault-movement intensity affect the seismic events that occur per unit of time. These faults divide larger layers into blocks that can be considered larger and longer faults. Conversely, thinner layers contain many faults, but of smaller

sizes, whereas thicker layers contain few faults, which are larger in size. Major recent earthquakes in Eurasia and their characteristics are shown in Table 1.

Table 1. Major earthquakes in Eurasia during the last five years and their characteristics.

Date	Latitude	Longitude	Depth	Mag (Mw)	dmin	rms	Place
27 July 2022	17.5601	120.8011	10	7	5.237	0.75	13 km SE of Dolores, Philippines
16 March 2022	37.7132	141.5793	41	7.3	2.936	0.88	57 km ENE of Namie, Japan
29 December 2021	−7.5482	127.5773	165.49	7.3	3.713	1.06	125 km NNE of Lospalos, Timor Leste
14 December 2021	−7.6033	122.2274	14.27	7.3	1.025	0.61	Flores Sea
11 August 2021	6.4748	126.7151	55.14	7.1	1.273	1.27	60 km ENE of Pondaguitan, Philippines
21 May 2021	34.5983	98.2513	10	7.3	4.655	0.77	Southern Qinghai, China
20 March 2021	38.4515	141.6477	43	7	2.378	0.75	30 km E of Ishinomaki, Japan
13 February 2021	37.7265	141.7751	43.98	7.1	3.085	0.94	73 km ENE of Namie, Japan
21 January 2021	4.9931	127.5145	80	7	2.821	0.77	211 km SE of Pondaguitan, Philippines
30 October 2020	37.8973	26.7838	21	7	1.518	0.59	13 km NNE of KarlovÃ¡sion, Greece
17 July 2020	−7.836	147.7704	73	7	1.671	1.1	114 km NNW of Popondetta, Papua New Guinea
25 March 2020	48.9638	157.6955	57.8	7.5	4.109	0.66	221 km SSE of Severo-Kurilâ, Russia
13 February 2020	45.6161	148.959	143	7	4.501	0.83	95 km ENE of Kurilâ, Russia
14 November 2019	1.6213	126.4156	33	7.1	1.271	1.15	141 km NW of Ternate, Indonesia

3. Data and Methodology

3.1. Data Acquisition

In this study, catalogues and descriptions of historical events were collected from the United States Geological Survey (USGS) and National Seismological Centre (NSC) ranging from 2000–2022. A database was developed using Landsat ETM+ data for regional faults, and the Geological Institute of the Russian Academy of Sciences (GIRAS) developed an active-fault database for Eurasia in the Laboratory of Neotectonics and recent geodynamics (Table 2). The database is composed of data from several sources, including studies published by several researchers [34,35]. This database is suitable for synthetically-active-fault analyses at a regional scale or large scale. An complete earthquake catalog alone is insufficient for risk estimation; however, data from several public and private organizations, such as the United States Geological Survey (USGS), Advanced National Seismic System (ANSS), Northern California Earthquake Data Center (NCEDC), and the National Earthquake Information Center (NEIC) were also collected. In this study, earthquake catalog, fault information from (GIRAS), digital elevation model (DEM), and lithology information from Landsat-8-image-and-USGS-based large-scale dataset were employed to train the GRU model, predict targets, and develop the SPM. The GEM published the earthquake hazard and risk atlas based on the traditional probabilistic seismic hazard assessment (PSHA) technique, which can be regarded as an authentic reference for validation of the integrated AI-based results. In the current research, a detailed seismotectonic map was developed for earthquakes stronger than 5.5 Mw, detailed faults, and geology in Eurasia. The above-mentioned information and maps were processed in the current study to generate thematic layers through digitization and georeferencing using ArcGIS Pro.

Table 2. Data used for earthquake-risk assessment in Eurasia.

Category	Thematic Layers	Source	Description of Data	Importance
Spatial-probability assessment (SPA)	Slope Elevation Curvature	Global digital elevation model (USGS) https://earthexplorer.usgs.gov/ (accessed on 20 February 2022)	Derived from Global ASTER DEM.	These factors control the landform, which may reform and activate crustal faults.
	Proximity to thrust Tectonic contacts	Geological Institute of the Russian Academy of Sciences (GIRAS) Global faults data	Derived from Landsat ETM+ and shapefiles using digitization and Euclidean distance ArcGIS.	High-magnitude events are observed in thrust faults; however, tectonic contacts does not necessarily generate earthquakes.
	Epicenter density Earthquake frequency Magnitude var Seismic gap Depth variation	USGS earthquake catalog (https://earthquake.usgs.gov (accessed on 20 February 2022))	Derived using kernel density and IDW interpolation using a complete catalog.	The occurrence probability can be understood through magnitude clusters, depth information on the fault zone, frequency of events, and gaps that are not yet affected.
	Geology	www.nrcs.usda.gov (accessed on 1 March 2022) Global soil data	Derived from Landsat 8 dataset.	Very solid granites are mostly found in fault zones that transmit energy better than others.
Earthquake-hazard assessment (EHA)	PGA	USGS global earthquake catalog (https://earthquake.usgs.gov (accessed on 20 February 2022))	PGA can be derived using (MMI = 1/0.3 × (log10 (PGA × 980) − 0.014) using Probabilistic approach, or it can be converted from MSK intensity, as presented in Table 3. $\log A\left(\frac{m}{s^2}\right) = 0.333 I_{msk} - 2.222$	Hazard is the temporal probability necessary for risk assessment.
Earthquake-vulnerability assessment (EVA)	Population density Public education	Global-risk-data Platformhttps://preview.grid.unep.ch/ (accessed on 10 March 2022)	Derived using digitization, kernel density, and IDW interpolation.	Social and physical characteristics/factors are necessary for the vulnerability assessment.
	High income level Gross-domestic-product value			
	Building density Industries			
Earthquake-risk assessment (ERA)	1. SPA × EVA 2. EHA × EVA	http://www.syque.com/quality_tools/tools/TOOLS11.htm, n.d. (accessed on 11 March 2022)	Derived using digitization, raster calculator, and various other tools.	Two main factors that are required for risk are the seismic hazard and the vulnerability of the population and property to this hazard.

Table 3. Conversion of MSK intensity to PGA.

MSK intensity to PGA conversion	Intensity in MSK scale	0	4	5	6	7	8	9	10	11	12
	PGA (in g)	0	0.03	0.05	0.092	0.18	0.32	0.52	0.82	1.2	1.6

3.2. Overall Methodology

In the current study, we developed a geo-database that contains thematic layers as the causal factors for the SPA (Figure 2). Numerical data points were generated in GIS using all the thematic layers, keeping the earthquakes and non-earthquakes as targets, and exported to an Excel file. The purpose of the integrated GRU–SRU approach is to provide a better understanding of multiple implementations of models and data. The GRU method has shown superior performance in predictions using huge datasets, and SRU can provide satisfactory accuracy for limited thematic datasets; hence, it was chosen for this study [36,37].

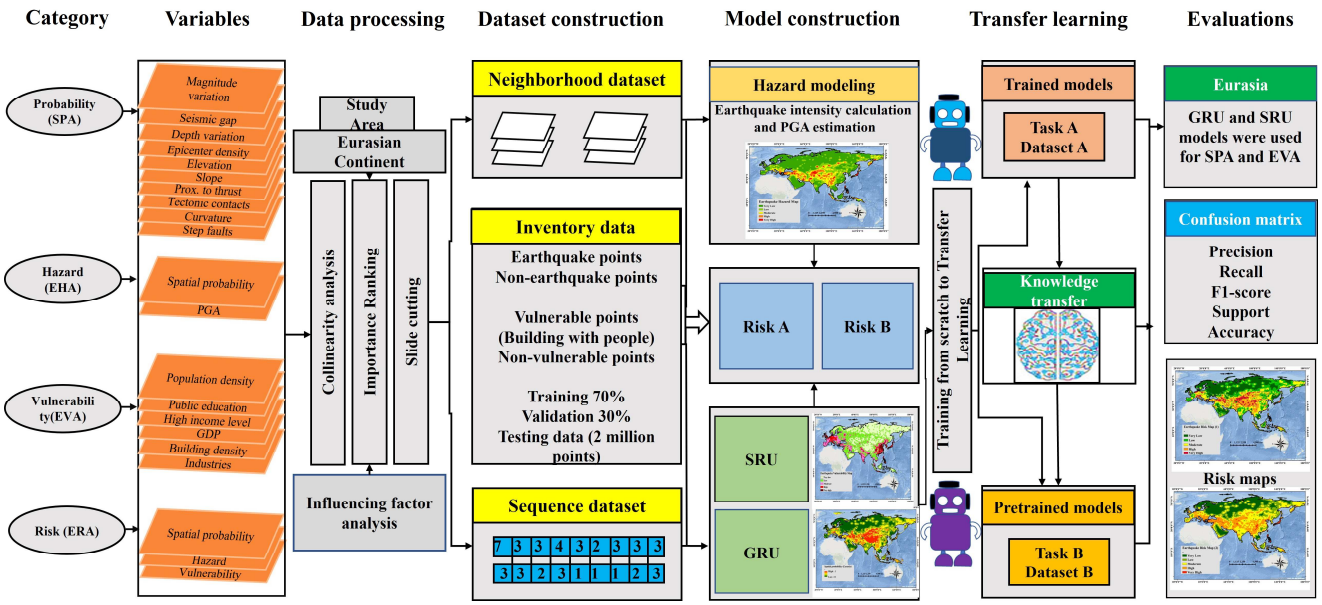

Figure 2. Methodological flowchart of earthquake-risk assessment.

It was first determined whether the probability assessment was important by correlating factors. Next, the GRU model was implemented for prediction purposes to estimate the earthquake spatial probability in Eurasia. Similarly, the vulnerability was estimated using the SRU model and several vulnerability factors, where targets were vulnerable (exposure) and non-vulnerable (bare land surface and unused land, desert, and forest areas) locations. The spatial-probability-prediction results were plotted with the density to check the prediction capability. However, an explainable AI, named SHapley Additive exPlanations (SHAP) [38], was implemented to estimate the probability based on individual instances for the prediction. Next, the interaction of the factors that described the logic behind the obtained prediction was plotted.

The predicted probability values were plotted for each factor to check how each factor contributed towards the SPA. Next, we estimated the PGA values using the MSK intensity and generated the earthquake-hazard map (EHM) for Eurasia. Finally, the risk was estimated by multiplying spatial probability by vulnerability (Risk A) and temporal probability (hazard) by vulnerability (Risk B). The risk maps were generated using a transfer-learning-based integrated GRU–SRU model, which was considered trustworthy, and maps were produced for future land-use planning and research purposes. The obtained risk maps were then compared with the GEM-based risk map for validation purposes. Ultimately, the Risk B map provided a greater closure output than the GEM-based risk map compared to the Risk A map.

3.3. Gated Recurrent Unit

The GRU is a simplified version of LSTM, and it is characterized by a smaller number of parameters than LSTM, according to Wang et al. [39]. The GRU model is very popular

due to its high accuracy with small data sets [40]. In the first step, GRU develops a single update gate by merging the input and forget gates in association with a reset gate. More status information can be brought in at the previous moment when the update gate value is larger. Similarly, the smaller the reset-gate value, the more information is neglected. Next, the update gate controls the degree of information of the preceding moment when brought to the ongoing state. The reset gate controls the degree of information of the previous moment by ignoring the status. Figure 3a illustrates a typical GRU architecture. The activation vectors are represented as r_t, z_t, and O_t at time t for the reset gate, update gate, and output gate, respectively. Mathematically, they can be expressed as:

$$Z_t = \sigma_g(W_z x_t + U_z h_{t-1} + b_z) \tag{1}$$

$$r_t = \sigma_g(W_r x_t + U_r h_{t-1} + b_r) \tag{2}$$

$$O_t = (1 - z_t) * h_{t-1} + z_t * \sigma_h \left(W_h x_t + U_h(r_t h_{t-1}) + b_h \right. \tag{3}$$

where sigmoid function is represented as σ_g and σ_h denotes the hyperbolic tangent. Here, W and U denote the parameter matrices, while b is considered the bias vector. The W_z, and W_r represent the parameter matrix with respect to update gate and reset gate, whereas W_h denotes the parameter matrix based on hyperbolic function.

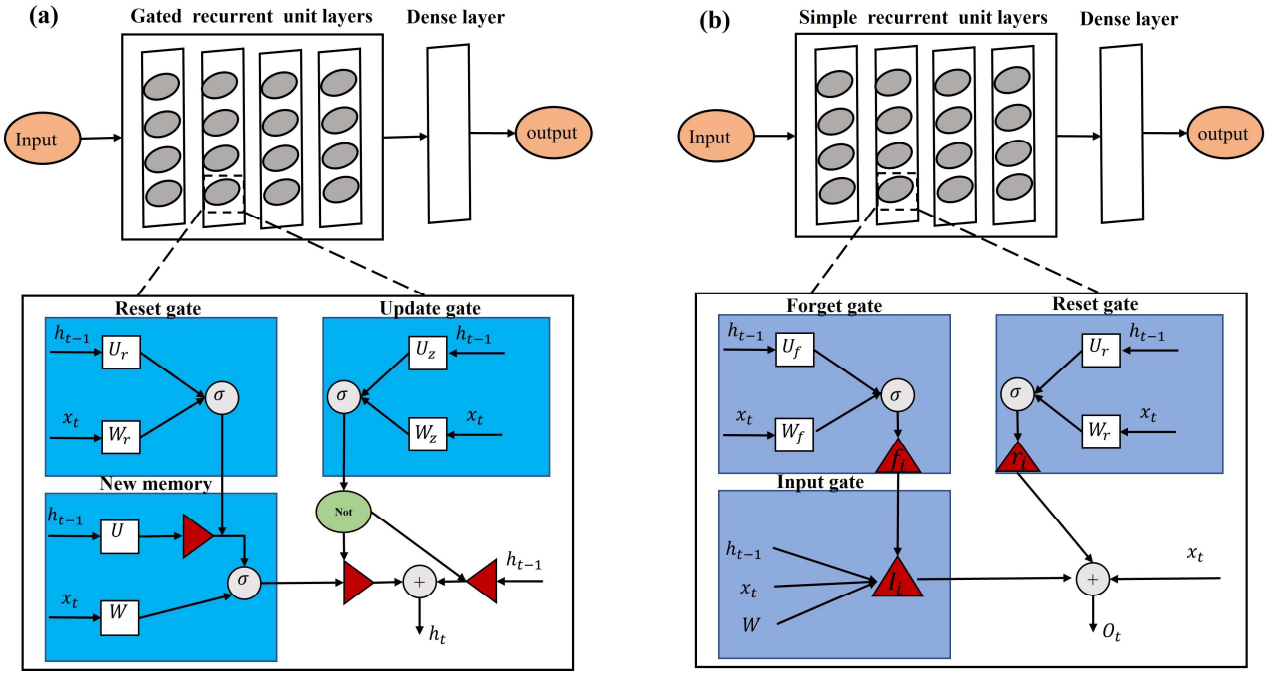

Figure 3. Architecture of deep-learning models: (**a**) GRU and (**b**) SRU.

3.4. Simple Recurrent Unit

The SRU model is the simple recurrent unit developed by Lei et al. [41] based on the LSTM and GRU models. The SRU model follows a similar gate structure to LSTM and GRU, which controls the information flow within the model. The gate calculations depend only on the current-input loop, which is the main principle of the SRU model. Therefore, the model only multiplies in a point-by-point matrix-dependent manner, which makes the network easy to adapt for running in a parallel process. The SRU model that sets the forget gate and reset gate is considered a deeper network, as it requires higher processing speed and less computational power. Figure 3b illustrates a typical SRU-model architecture. The

activation vectors at time t, such as f_t, r_t, I_t, and O_t, represent forget gate, reset gate, input gate, and output gate, respectively. They can be mathematically expressed as follows:

$$h_t = \sigma\left(W_f x_t + U_f \odot h_{t-1} + b_f\right) \quad (4)$$

$$I_t = f_t \odot h_{t-1} + (1 - f_t) \odot (W x_t) \quad (5)$$

$$r_t = \sigma(W_r x_t + U_r \odot h_{t-1} + b_r) \quad (6)$$

$$O_t = r_t \odot h_t + (1 - r_t) \odot x_t \quad (7)$$

where the point-wise multiplication operation is represented as $\odot$, while W and U are parameter matrices and b is the bias vector [42].

3.5. Data Preprocessing and Feature Engineering

In this study, we selected 11 thematic layers (slope, elevation, curvature, proximity to thrust, tectonic contacts, epicenter density, earthquake frequency, magnitude variation, seismic gap, depth variation, and geology) to implement the GRU predictive model for SPA. The earthquake data collected from USGS and randomly generated non-earthquake data were trained using the GRU-based binary classification model. Multiple raster and vector datasets from GIRAS and other agencies were utilized for the preparation of thematic layers, which were then converted into multi-values and incorporated into the training process. First, the data were prepared in an Excel sheet with all factors and the binary target of earthquakes and non-earthquakes (Figure 4). Second, the GRU model continuously scanned through the input dataset to predict the earthquake (1) and non-earthquake (0) data points. The classifier was trained with 70% (training) and 30% (validation), randomly. During training, 31,383 samples were prepared using the above-mentioned dataset for training and validation purposes. Third, the test was conducted with 2 million points to derive the SPA. The model parameters that were used to predict and optimize the model included Adam optimizer, batch size (100), and verbose (1). Finally, predicted values were converted into pixels after post-processing and the SPM was generated. As a result, the SHAP was implemented to explain the prediction outputs, as well as factor-interaction values.

In the next step, the SRU model was developed as a binary classification for the earthquake-vulnerability assessment [42]. Next, six parameters were selected as inputs to feed the model in a sequence with a random split of the dataset (70% training and 30% validation) (Figure 4). Subsequently, the SRU model continuously scanned through the input dataset to predict the vulnerability (1) and non-vulnerability (0) datapoints. During training, the 31,703 samples were prepared using the above-mentioned dataset for training and validation purposes. Finally, the test was conducted with 2 million points to derive the EVA. To optimize the SRU, the Adam optimizer was employed, while the other model parameters included the batch size (64), epoch (100), and loss function (0.001).

The hazard map was developed based on GRU-based probability and MSK intensity for the Eurasian continent. The MMI intensity was calculated by converting magnitude to intensity values. It is evident that the MMI scale is similar to MSK intensity (Table 3), with 12 classes; therefore, we converted the MSK intensities into PGA values. Next, the IDW interpolation technique was implemented to make the PGA variation [43]. Next, the Venn-diagram-intersection theory was employed to develop a hazard map, and the zones were derived using the quantile classification technique [44]. Finally, the risk was estimated using all the above-mentioned components.

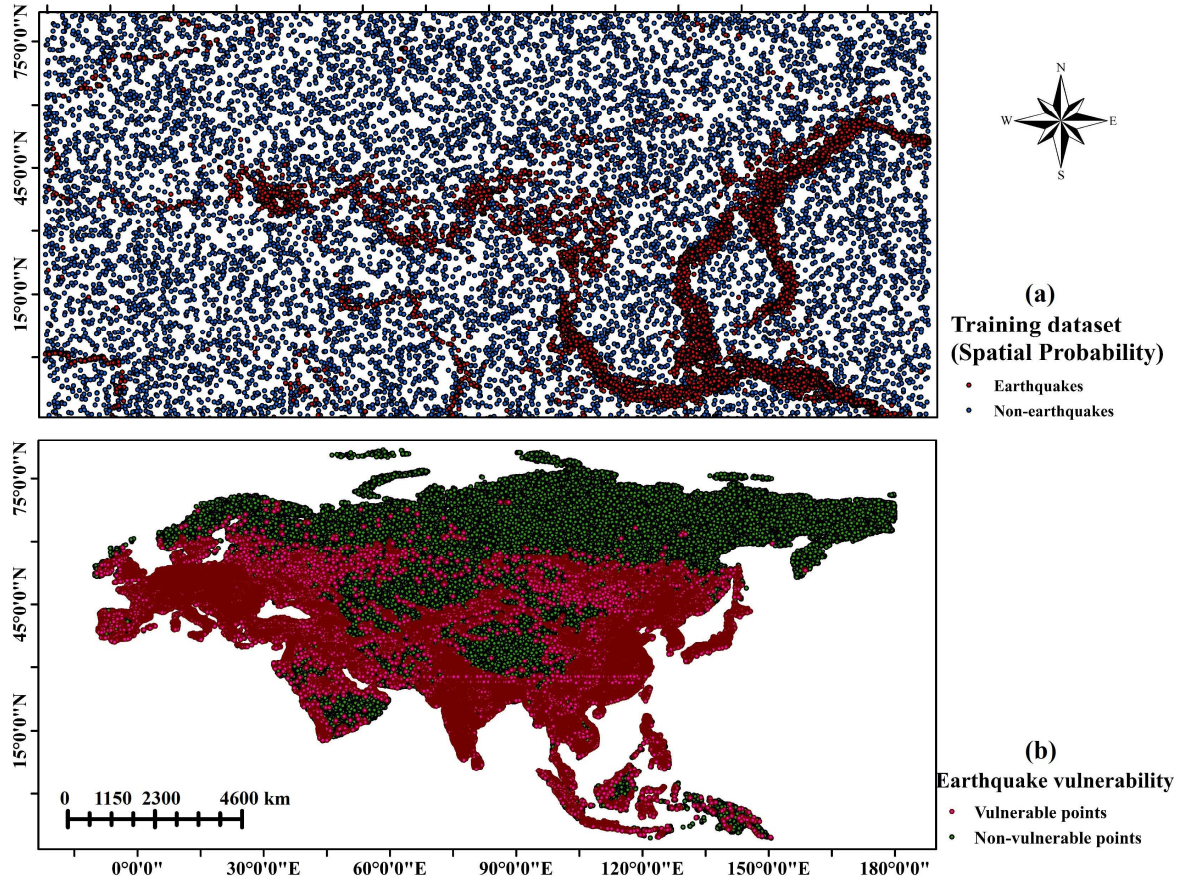

Figure 4. Training dataset for earthquake-probability-and-vulnerability assessment. (**a**) Earthquakes (red) and non-earthquakes (blue) and (**b**) vulnerable points (red) and non-vulnerable points (green).

3.6. Data Representation

For both GRU and SRU models, the layers were sequentially stacked as single-band images by converting them into data points in an Excel file. The SHAP model was implemented to rank the parameters based on their importance. The series of parameters was as follows: magnitude variation, depth variation, tectonic contacts, seismic gap, earthquake frequency, epicenter density, elevation, slope, proximity to step faults, proximity to thrust faults, curvature, and geology. Each pixel value of structured data was converted based on the sequence of significance in descending order. Hence, the most important parameters were processed first, followed by the least important parameters. The recurrence structure of both models, GRU and SRU, allows important information that contributes to vulnerability to be retained and passed to the hidden layer. The importance of factors is shown in Figure 5a, using a summary plot and the effect. Figure 5b depicts the correlations among the four most important factors used for spatial probability. The highest correlation values were observed between magnitude variations and seismic gap and between magnitude variation and depth variation.

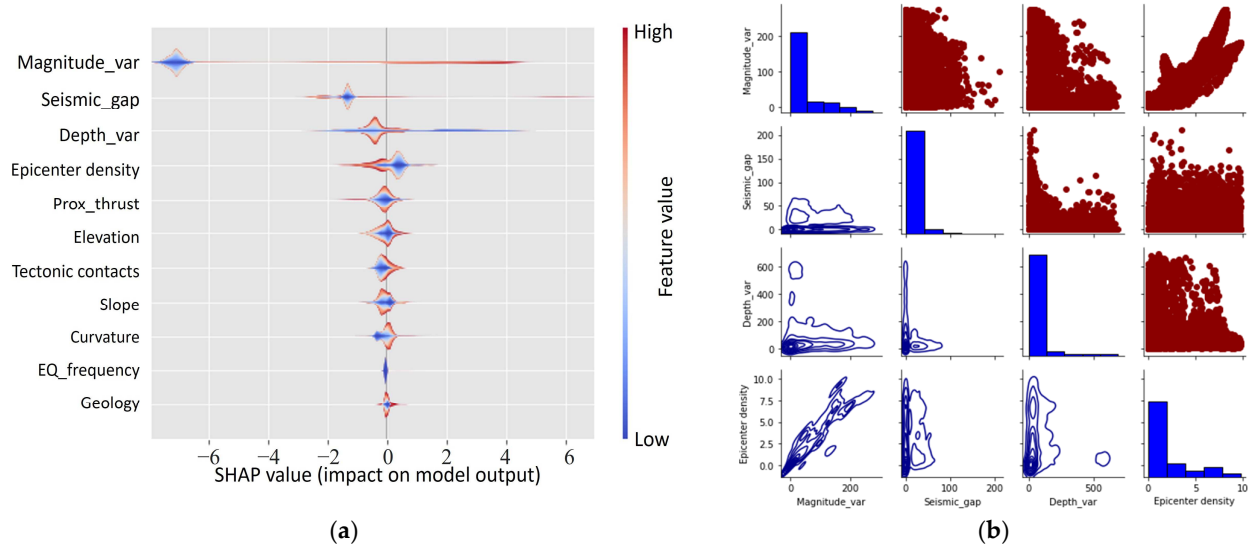

(**a**) (**b**)

Figure 5. (**a**) Factors' importance and impact on model output. (**b**) Correlations among four most important factors.

3.7. Transfer Learning

Transfer learning deals with the transfer of gained knowledge from a pre-trained model to new scenarios (Figure 2). According to Pan and Yang [45], it is characterized by a source domain (DS), a target domain (DT), a learning task (TS), and a target learning task (TT). Tan et al. [46] further explained the transfer-learning task by domain, tasks, and a non-linear function of deep neural networks. In the case of network-based deep transfer learning, the parameters of the source model are generally used in the target model [47]. In the target model, these parameters are considered new initial values and applied to a new dataset. Tuning a network is faster and easier in the case of transfer learning than when training another model from scratch. Transfer learning can perform satisfactorily using fewer data.

Firstly, a GRU model was trained using the earthquake catalog in and around Eurasia. Secondly, the pre-trained model was tested using another dataset without any targets to predict information. The dataset was developed for Eurasia with 2 million points to estimate the spatial probability using the knowledge gained from the trained model. Similarly, an SRU model was trained using vulnerable and non-vulnerable points as targets. Another dataset was developed with 2 million points without any targets to predict the information to estimate the vulnerability using the knowledge gained from the previously trained model. With transfer learning, SPA cannot be restricted to a specific location. Instead, the knowledge of SPA from a data-rich area can be shared and utilized by others, which is an asset for SPA in new regions, especially areas with limited/no data. Furthermore, this can be useful in AI-based vulnerability assessments. Thus, to validate the transfer learning, we applied transfer learning for both GRU and SRU models in the context of spatial-probability and -vulnerability assessments in Eurasia, with great accuracy.

3.8. Evaluation Metrics

In the current study, we applied 11 factors for SPA and 6 factors for EVA, which were derived as thematic layers from seismological, geological, and geo-structural, sociological data as factors (Table 2). The performance-evaluation metrics employed to appraise the predictive dimensions were as follows: recall (TPR), F_1-score (F_1), precision (PPV), and support and accuracy (ACC) [48]. The statistical expression of these metrics is presented in Equations (8)–(11).

$$TPR = \frac{TP}{P} = \frac{TP}{TP + FN} = 1 - FNR. \quad (8)$$

$$F_1 = 2 \times \frac{PPV \times TPR}{PPV + TPR} = \frac{2TP}{2TP + FP + FN}. \quad (9)$$

where TPR (hit rate) represents true-positive rate, while F_1-score denotes the harmonic mean of precision and sensitivity. The precision and accuracy must be expressed as:

$$PPV = \frac{TP}{TP + FP}. \quad (10)$$

$$ACC = \frac{TP + TN}{P + N}. \quad (11)$$

where PPV denotes the positive predictive value and ACC is the accuracy. Here, N and P demonstrate the negative and positive data points, respectively, where TN is true negative, FP is false positive, and TN is true negative.

4. Results

4.1. Spatial-Probability Assessment

The spatial-probability assessment (SPA) was performed using the GRU model based on the classifications of the earthquake (1) and non-earthquake (0) points. In total, 31,383 points were derived using various factors, of which 15,700 were earthquakes above 4.5 Mw, while 15,800 were non-earthquakes. The GRU model predicted 11,941,030 km^2 as the most probable earthquake location in Eurasia. The GRU model recorded 93.17% accuracy for the SPA. The precision was estimated as 0.93, the recall was 0.93, the F1 score was 0.93, and the support was 9415. The SPM is shown in Figure 6. The density of the probability is plotted; according to this information, the model predicted more values for the earthquakes than the non-earthquakes (Figure 7a).

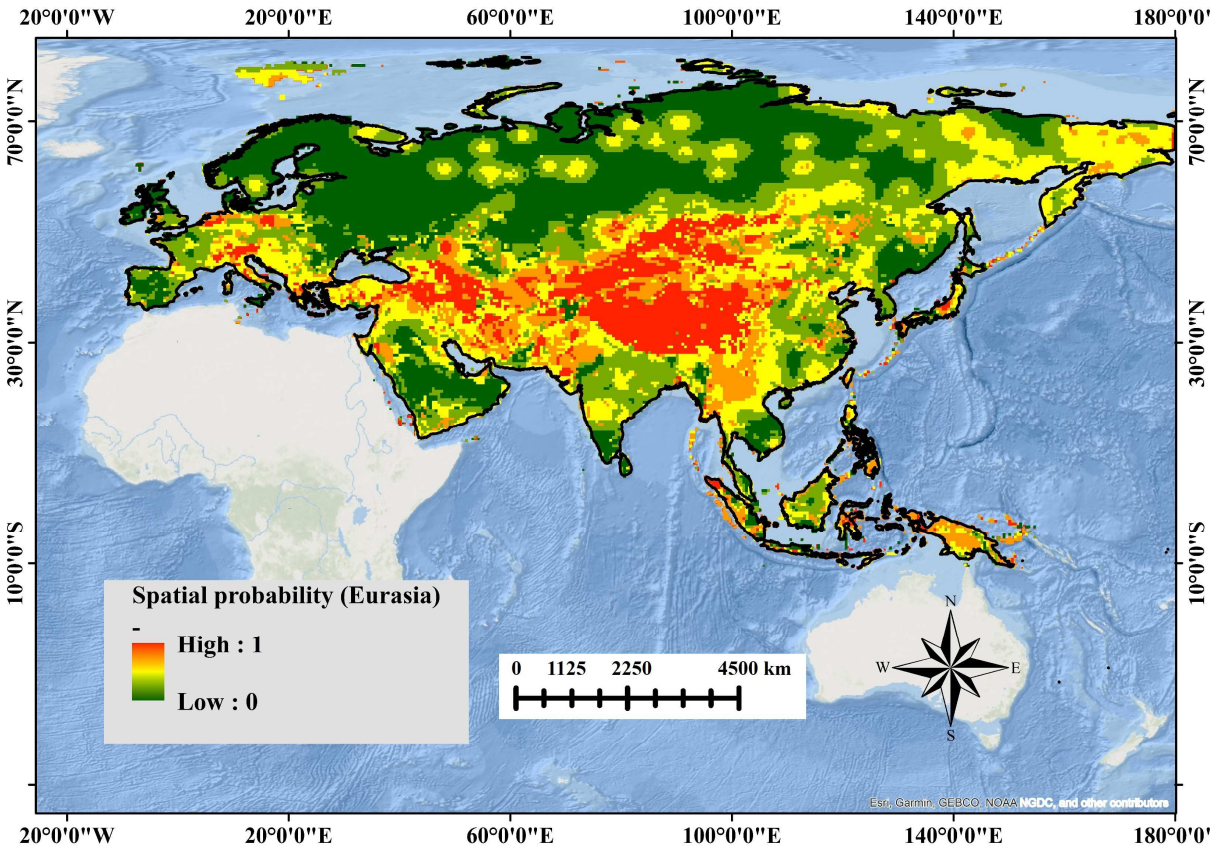

Figure 6. Earthquake-spatial-probability map (SPM) developed using the GRU model.

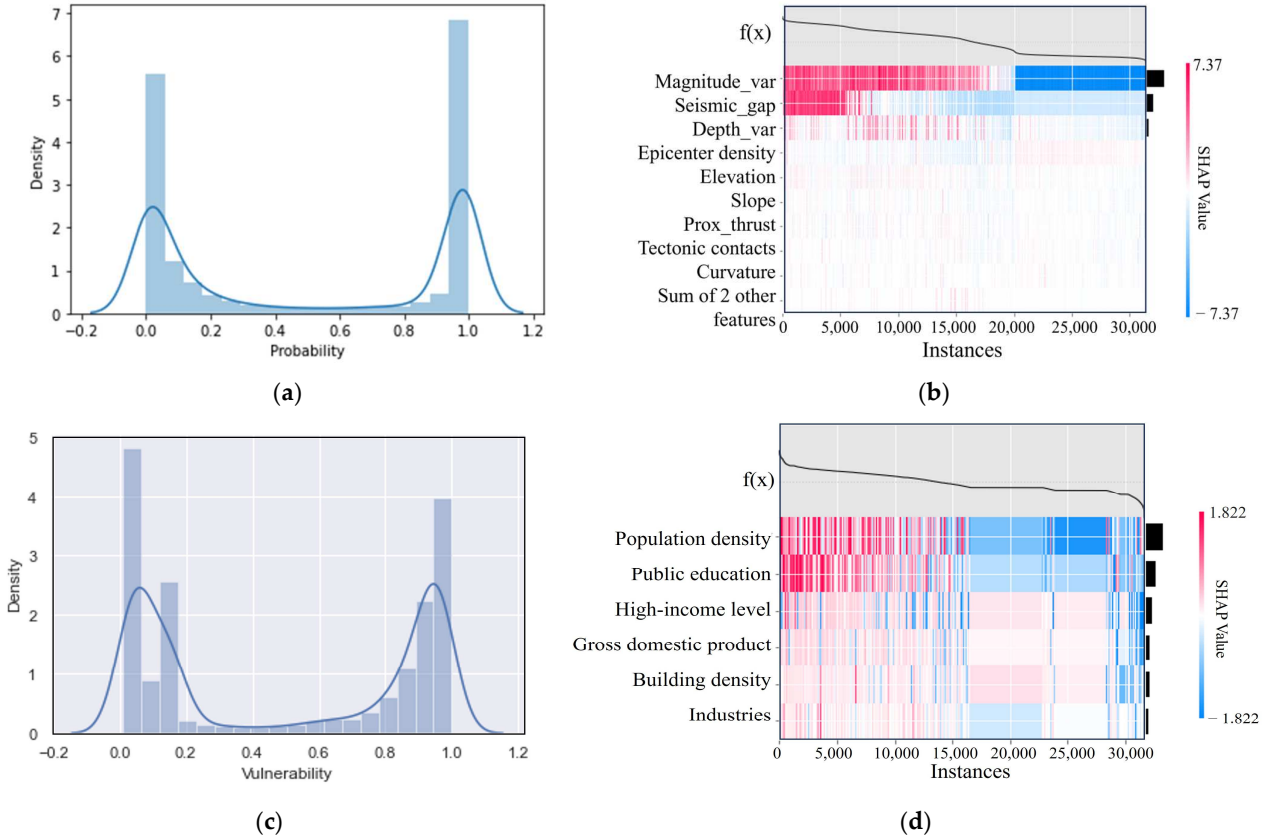

Figure 7. Estimation of: (**a**) spatial-probability density, (**b**) importance of factors, (**c**) spatial-vulnerability density, and (**d**) importance of factors.

The importance of all the applied factors is presented in Figure 7b. The values ranging between 0 and 0.2 were considered to represent low probability, while the values ranging between 0.8 and 1 were considered to represent high probability. According to the Shapley game theory, the highly important factors are magnitude variation, seismic gap, depth variation, and epicenter density.

Three factors, magnitude variation, seismic gap, and depth variation, contributed more towards earthquake prediction than non-earthquake prediction. No discernible patterns were observed in any of the unpredicted earthquakes. The probability map was derived with probability values ranging from 0 (non-earthquake) to 1 (earthquake). The model accuracy and loss are plotted in Figure 8a,b and the classification report is shown in Table 4. More than 13,000 earthquakes fell within the high-probability zone, which was mostly restricted to the vicinity of the active fault locations in the Alpine–Himalayan belt and Pacific Ring of Fire. The high-probability zones were characterized by high levels of earthquake magnitude, fault density, epicenter density, and seismic gap.

The future probability of earthquake occurrence is higher in the Alpine-Himalayan Belt and the countries situated near to Pacific Ring of Fire, as shown in Figure 6. However, the Alpine-Himalayan Belt has already experienced moderate (4.5 Mw) to disastrous magnitude events (8 Mw) due to the collision zones and thrust faults. Most of the earthquakes in this area are deep-focus earthquakes. The Pacific Ring of Fire is characterized by thrust faults and volcanic activities producing a huge number of earthquakes. These zones have a high capability to strike high-magnitude earthquakes in the future.

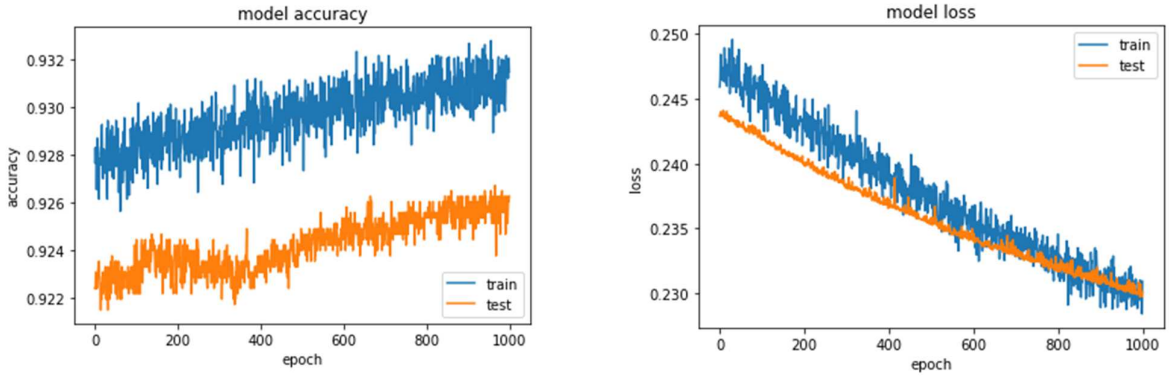

(**a**) (**b**)

Figure 8. (**a**) Accuracy and (**b**) model loss for the GRU model.

Table 4. Model evaluation report for GRU model.

		Precision	Recall	F1 Score	Support
GRU report (Prediction accuracy: 0.931705)	Non-earthquake	0.9422	0.9186	0.9302	4666
	Earthquake	0.9219	0.9446	0.9331	4749
	Accuracy			0.9317	9415
	Macro average	0.9320	0.9316	0.9317	9415
	Weighted average	0.9320	0.9317	0.9317	9415
	Confusion matrix	True positive		True negative	
	Predicted positive	4286		380	
	Predicted negative	263		4486	

Few high magnitude-earthquakes can also be found out of these zones in Eurasia, specifically due to large local active faults. The above-mentioned zones are characterized by the interdigitation of rocks, which makes the zones irregular with complex geo-structures and deformation. Few seismic gaps can be found in the map that shows high probability. Medium probability could be observed in the surrounding areas of high probable zones. Russia, Eastern China, Central and South India, Saudi Arabia, and Western Europe are falling under low probability zone. Countries falling under high probability are Central Europe, Turkey, Iran, Syria, Iraq, Pakistan, India, West China, Nepal, Bhutan, Bangladesh, Myanmar, Indonesia, and Japan.

4.2. Hazard Evaluation

Earthquake hazard for the Eurasian continent was developed that involves a source of strong vibration zones. Ground-motion footprints in terms of PGA were estimated using the MSK intensity-PGA conversion as shown in Table 3. Using the PGA values and spatial probability, the hazard map was developed through GIS. The degree of earthquake hazard in Eurasia was developed where PGA reached to a minimum of (0.0276–0.115 g) or more and could be appraised as a hazardous zone. The developed hazard map is shown in Figure 9. The intensity is very high in the countries such as Japan, Indonesia, Bhutan, Myanmar, North India, Pakistan, Iran, Turkey, and central Europe.

Other countries in Eurasia are coming under low to medium category. Next, the hazard map was classified into five classes: very-high (>IX), high (VIII–IX), moderate (VI–VIII), low (V–VI), and very-low (<VI). The obtained map demonstrates that approximately 24,940,772 km^2 of Eurasia is falling under a very-high hazard zone. Most of these areas are located in the Alpine Himalayan belt and Pacific Ring of Fire while the northern part of Eurasia (Russia and neighboring countries) is coming under the low to the very low zone. There is a hazard zone can be observed from Pakistan towards Russia followed by Afghanistan, Tajikistan, Kirgizstan, Kazakhstan, and Mongolia. However,

the entire Himalayan zone is covered by moderate to very-high hazard zones as per the obtained results.

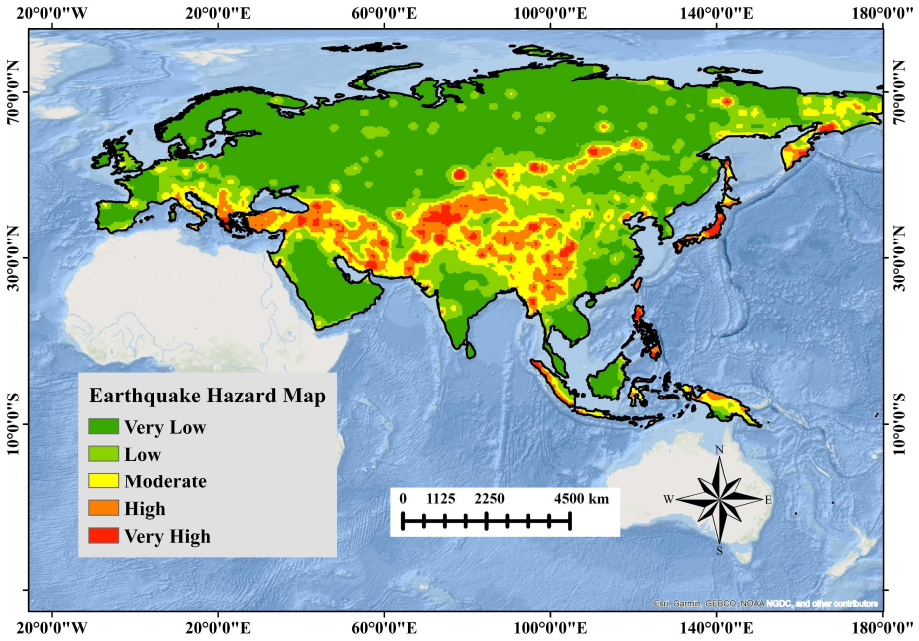

Figure 9. Earthquake hazard map (EHM) for Eurasia.

4.3. Vulnerability Assessment

The earthquake vulnerability map of the Eurasian continent was developed using 6 parameters. The vulnerability map generated based on the deep SRU model as shown in Figure 10. Population density (24.9%), public education (19.2%), high-income level (15.2%), GDP (14.7%), building density (14%), and industries (12%) were ranked as 1 to 6, respectively. The lowest rank was obtained by a number of industries, whereas the remainder were ranked higher. The model achieved an overall accuracy of 89%, whereas precision (0.89), Recall (0.89) and F1 score (0.89) were achieved by vulnerability prediction (Table 5). The model accuracy and model loss are presented in Figure 11a,b. The reason behind the higher testing accuracy than training could be the transfer learning with a new data set. The obtained vulnerability map was classified into five classes based on the quantile classification technique: very-low, low, medium, high, and very-high. The resulting map shows that approximately 15,801,480 km^2 area of the continent is under the very-high vulnerability zone.

Table 5. Model evaluation report for SRU model.

		Precision	Recall	F1 score	Support
SRU Report	Non-vulnerability	0.8959	0.8908	0.8933	4771
	Vulnerability	0.8907	0.8958	0.8932	4740
	Accuracy			0.8933	9511
	Macro average	0.8933	0.8933	0.8933	9511
	Weighted average	0.8933	0.8933	0.8933	9511
	Prediction accuracy: 0.89				

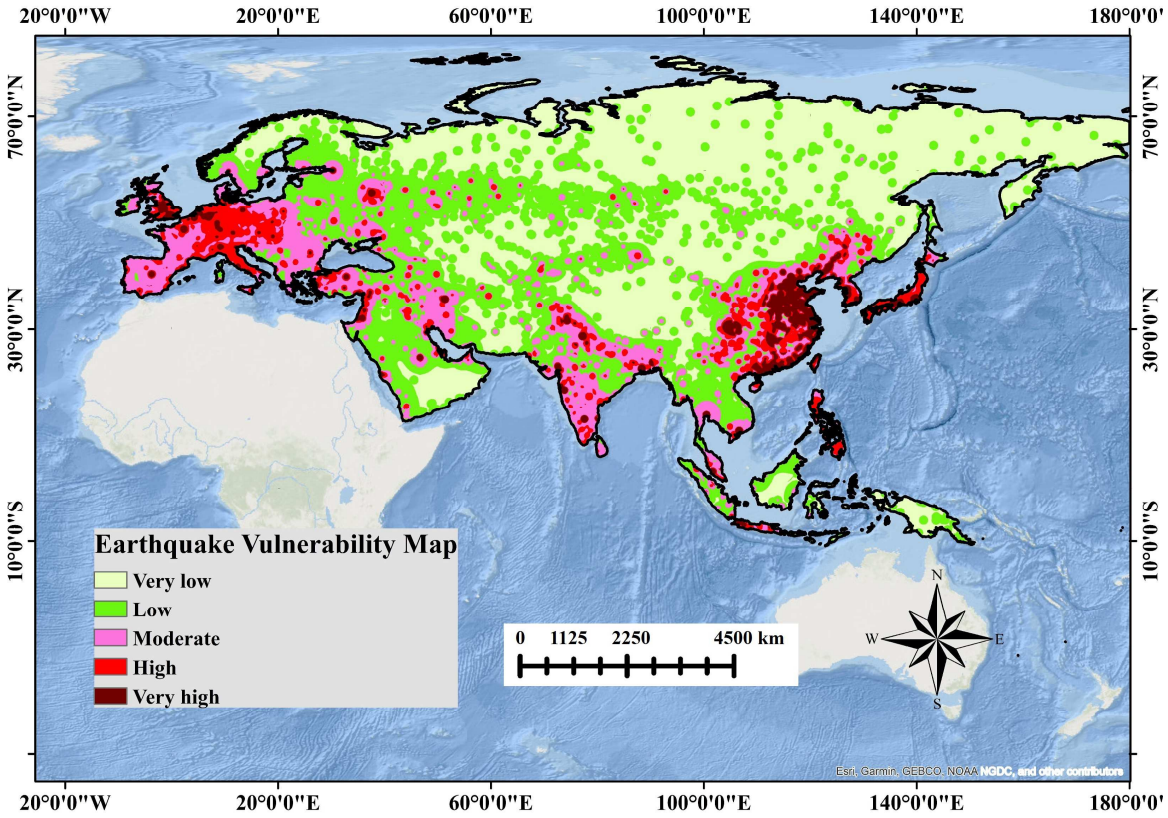

Figure 10. Earthquake vulnerability map for Eurasia based on SRU model.

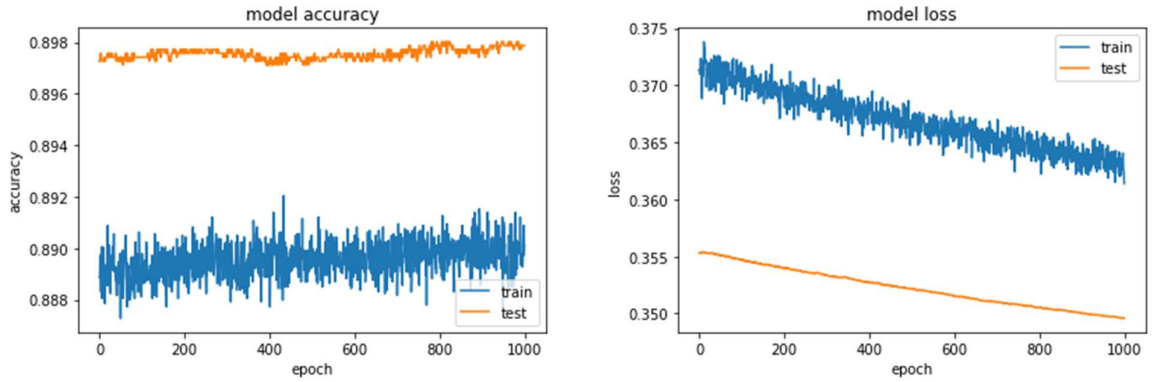

(**a**) (**b**)

Figure 11. (**a**) Accuracy and (**b**) model loss for the SRU model.

The density of the vulnerability was plotted where the model predicted more values for the non-vulnerable points than for the vulnerable points, which resulted in a low accuracy, of 89% (Figure 7c). The importance of all six factors (Figure 7d) demonstrates the instance-wise SHAP values. Several parts of the Eurasian continent fall within the very-high-vulnerability zone. These are Central Europe, Central Eurasia, and Western Eurasia. Japan, Korea, China, Indonesia, India, Iran, Turkey, and Europe possess high seismic vulnerability under the present seismic scenario. Russian, Georgian, Mongolian, Azerbaijani, Turkmenistan, Afghanistan, Tajikistan, Uzbekistan, and Kazakhstan are countries within the moderate-to-low-vulnerability zone, characterized by a moderately low vulnerability index. Therefore, the resultant map is useful for the vulnerability mapping of 93 countries in Eurasia.

4.4. Risk Estimation

The earthquake risk was spatially evaluated using the integrated AI and transfer-learning technique, as presented in Figure 12. Two risk maps were developed, Risk A and Risk B, and classified using quantile classification techniques. In this study, the risk was classified into five classes, very high, high, moderate, low, and very low, for both maps. According to the obtained outputs, 6,345,693 km^2, 8,881,332 km^2 and 1,697,867 km^2, and 15,840,672 km^2 of the Eurasian continent was regarded as a very-high-to high-risk zone based on the Risk A and Risk B maps, respectively (see Table 6).

Table 6. Risk-area calculation for Eurasia using an integrated AI model.

	Classes	Area (S. km)	In (Hectares)	Possible locations
Risk A	Very high	6,345,693	6,345,693,00	Central Eurasia, including Japan, Indonesia, China, India, Pakistan, Iran, Turkey, and some parts of Europe.
	High	8,881,332	8,881,332,00	Areas surrounding Alpine–Himalayan Belt
	Moderate	8,997,807	8,997,807,00	Northern and Southern Eurasia
	Low	22,535,100	22,535,100,00	
	Very low	8,000,068	8,000,068,00	
	Total	**54,760,000**	**54,760,000,00**	
Risk B	Very high	1,697,867	1,697,867,00	Alpine–Himalayan belt, including Japan, Indonesia, China, India, Pakistan, Iran, Turkey, and Southern Europe.
	High	15,840,672	15,840,672,00	
	Moderate	18,337,150	18,337,150,00	Northern and Southern Eurasia
	Low	13,884,300	13,884,300,00	
	Very low	5,000,011	5,000,011,00	
	Total	**54,760,000**	**54,760,000,00**	

Finally, 8,997,807 km^2 and 18,337,150 km^2 of Eurasia were at moderate risk on both maps. The very-high-risk areas were observed in central Eurasia, including Japan, Indonesia, China, India, Pakistan, Iran, Turkey, and some parts of Europe. Medium-to-very-low risk was found in northern and southern Eurasia (Figure 12). Most of the future casualties or damages are expected in the very-high-risk zone, where a pancake form of collapse may occur [49]. The current risk results indicate that aged buildings, high population density, low income, and low GDP could be the reasons for the high risk estimated for this area. Furthermore, the risk results suggest that the renovation and rehabilitation of aged buildings in high-population-density areas is a primary requirement. Both low- and very-low-risk zones might be unaffected by any future damage, and if this damage occurs, it can be repaired. The total population in very-high-to-high-risk areas in Eurasia is estimated to be in the range of approximately 1.5 billion, and approximately USD 11,250 million in Eurasia is at high risk from earthquake scenarios in the Alpine–Himalayan belt and the Pacific Ring of Fire.

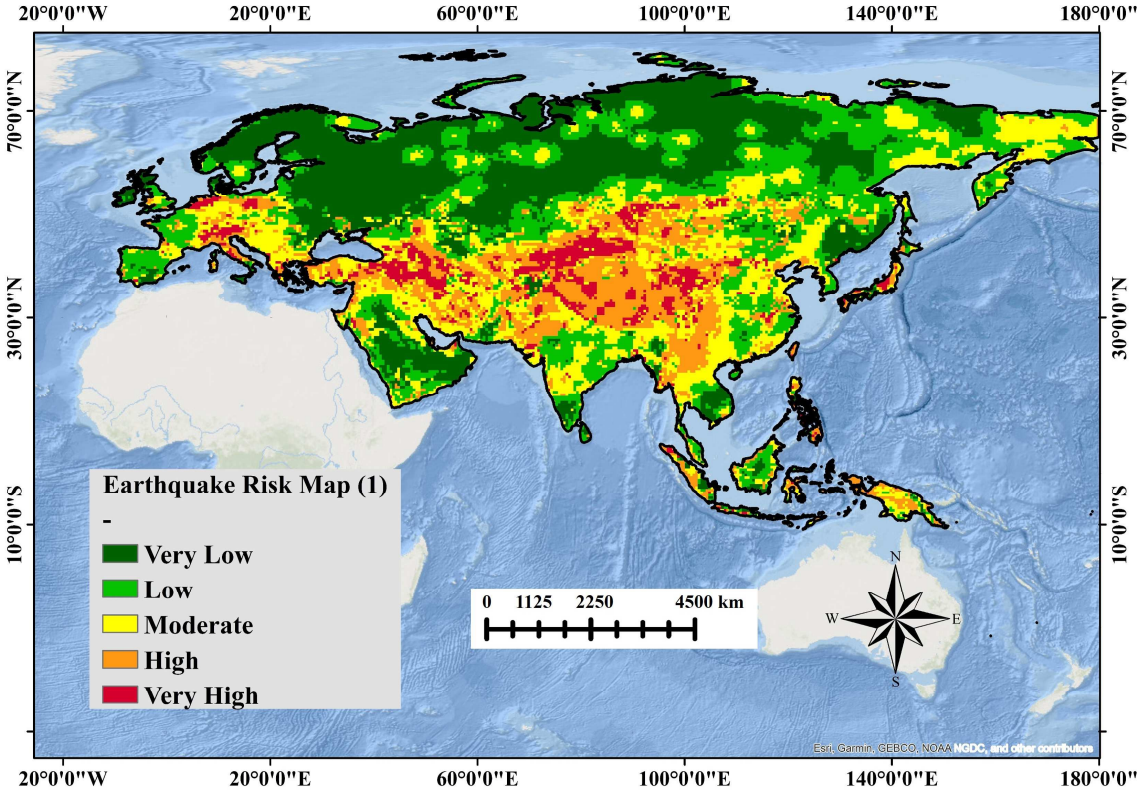

(**a**)

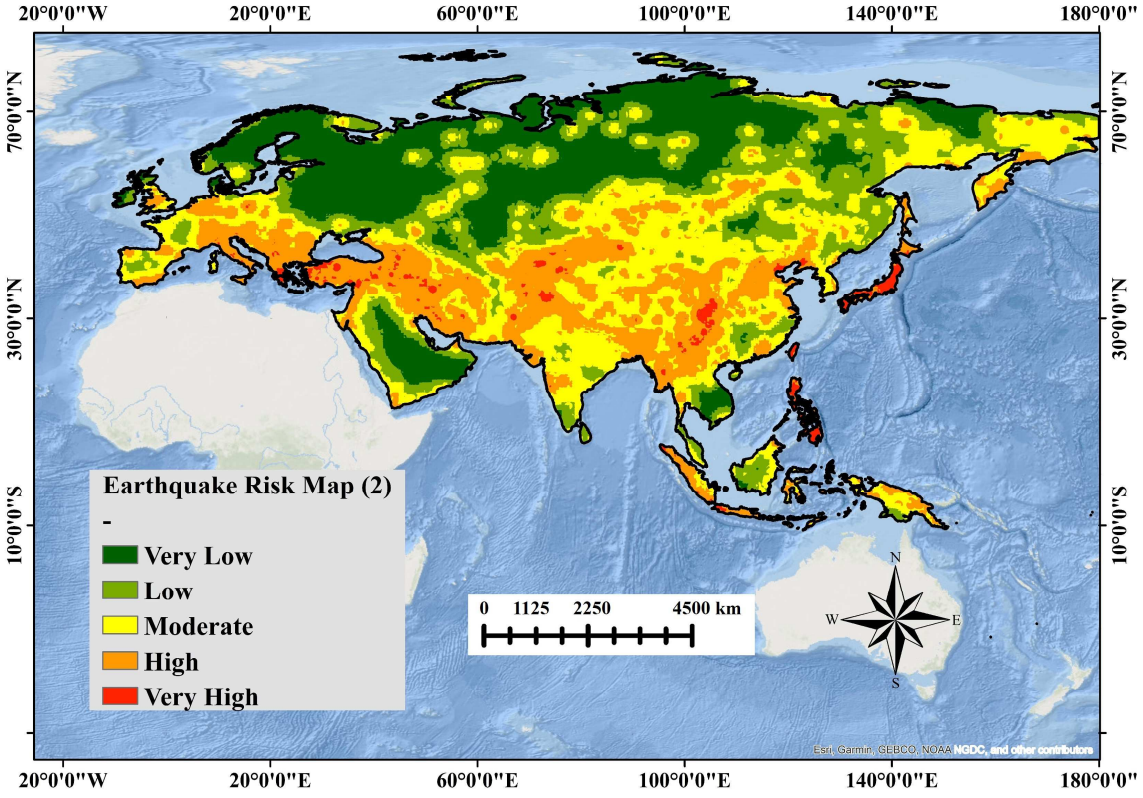

(**b**)

Figure 12. Earthquake-risk map for Eurasia based on two approaches: (**a**) Risk A AND (**b**) Risk B.

5. Discussion

The earthquake spatial probability was evaluated for Eurasia using a deep GRU model to achieve robust accuracy. The most recent knowledge on seismic activity and geospatial data in Eurasia was employed to estimate the earthquake probability. This study compared the old probabilistic seismic-zoning map and the latest earthquakes in Eurasia with the resulting earthquake-probability map. The development of a probability-assessment model for earthquakes above 5.5 Mw using several conditioning factors was a major objective, and excellent results were shown. The prime cause the very high spatial probability in Central Eurasia could be the major active faults and the huge number of high-magnitude earthquakes. According to the literature, the GRU model is one of the most reliable models for prediction. In this study, the GRU achieved an accuracy of 93% and significantly reduced the processing time, as well as improving the efficiency. The proposed model provides the best estimates of probability using historical earthquakes. The interaction values for each factor showed that the four highest-ranking factors (magnitude variation, seismic gap, depth variation, and epicenter density) indicated positive interaction, whereas zero and negative interactions were shown by other factors (Figure 13). The interaction effects were already doubled in the pairwise interaction plot. The SHAP values were higher in the main effects (diagonals) than in the interaction effects (off-diagonals). Most of the earthquakes were predicted by the model at depths of 0–200 km, with a magnitude variation of 5.7–8 Mw, a seismic gap of 0–100 km, and an epicenter density characterized by 0–10 events (Figure 14). Because the GRU model generates spatial probability, the probability classes explain the variation in the probability with respect to distance and location. The current study shows good accuracy using GRU, as mentioned above, which is comparable to some DL-based approaches to spatial probability, as discussed below. Jena et al. [50] conducted a spatial-probability study for India using a deep convolutional neural network (DCNN) and successfully estimated the probable areas. They achieved an overall accuracy of 96%. Pourghasemi et al. [9] conducted a multi-hazard-probability assessment study in Iran, in which they estimated the spatial probability of earthquakes with an accuracy of above 80%. Finally, they developed a multi-hazard map that works as a primary tool for sustainable land-use planning.

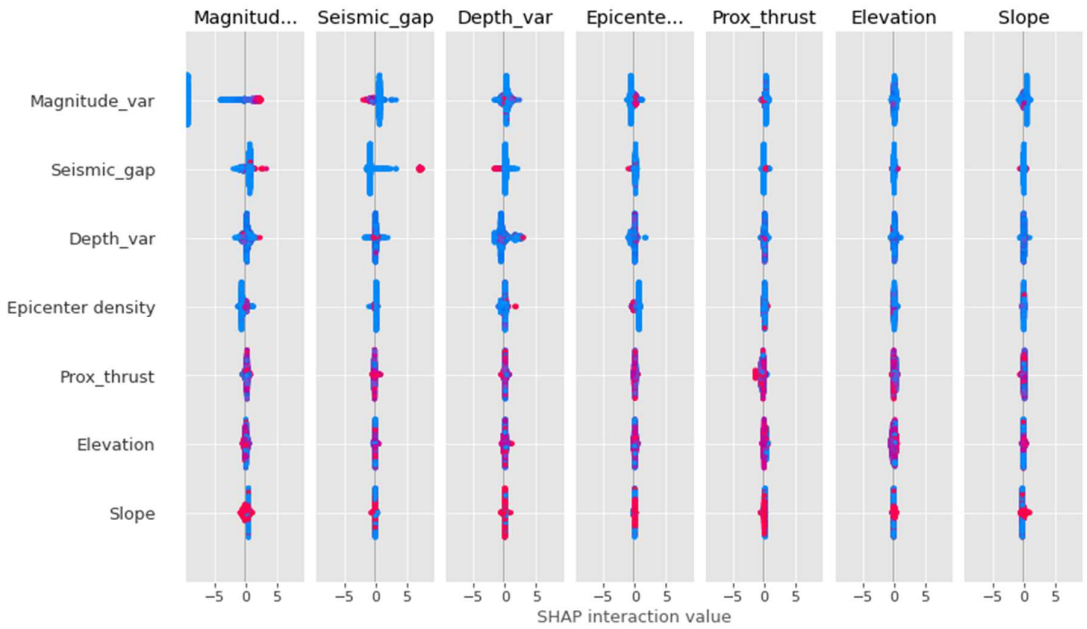

Figure 13. Correlations among factors based on their interaction values.

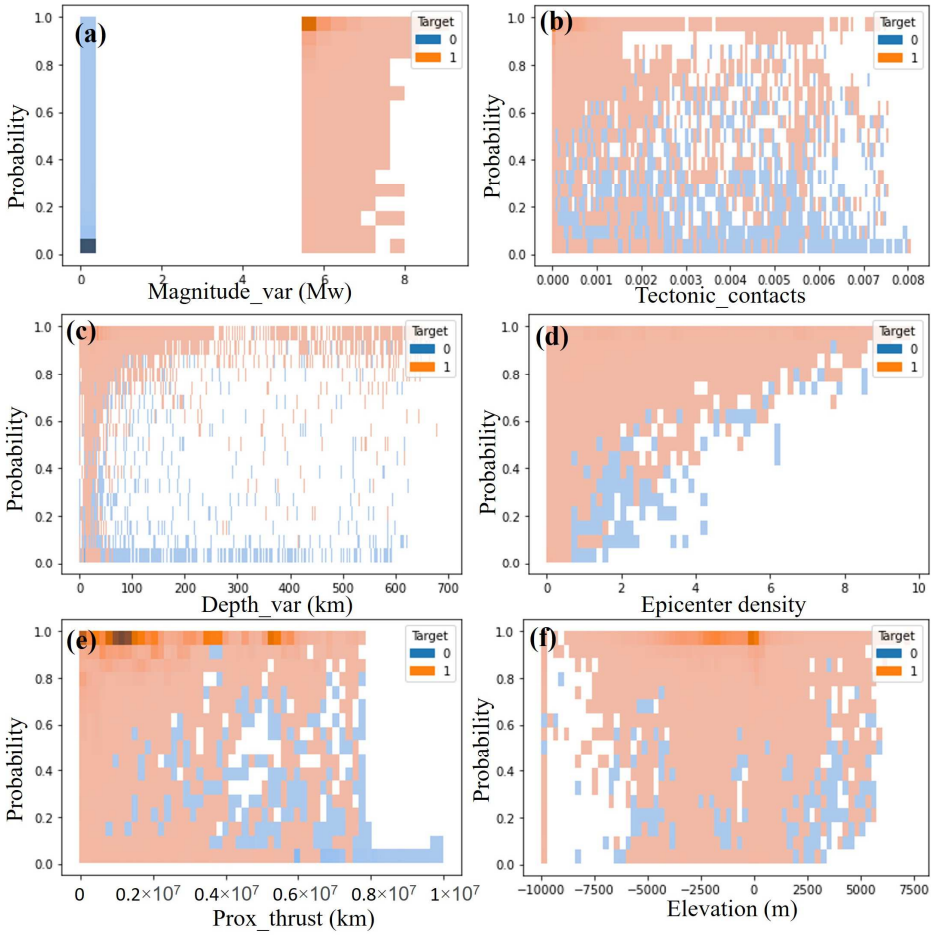

Figure 14. Each factor's contribution towards SPA. (**a**) Magnitude variation, (**b**) tectonic contacts, (**c**) depth variation (km), (**d**) epicenter density, (**e**) proximity to thrust, and (**f**) elevation. (0-non earthquake and 1-earthquake).

The earthquake hazard was estimated using the PGA values of the macro-seismic events. The MSK intensities were estimated for all the earthquakes above 5.5 Mw and converted into PGA values. The SPM was multiplied by the PGA to estimate the EHM. This hazard map can suggest the level of destruction that may occur due to high-intensity earthquakes. Therefore, according to the MSK intensity scale, it can be assumed that an earthquake intensity > IX is destructive and catastrophic, and that the hazard is very high. Intensity ranges between VIII and IX can be considered to denote highly hazardous zone, VII–VIII denote medium-hazard zones, V–VII denote zones with low levels of hazard, and values of <V denote zones with very low hazards. The hazard map was prepared based on the quantile classification in GIS. Very-high-to-high hazards were observed in the Himalayan belt and in the Eurasian countries in the Pacific Ring of Fire. The resulting map showed very low hazards in northern and southern Eurasia and can be used for disaster prevention and land-use-planning services by administrative agencies. The very-high-to-high hazard levels may be due to seismic amplification in loose sedimentary rocks, active faults, and complicated geo-tectonics. Abdollahzadeh et al. [51] conducted a PSHA by considering potential seismic sources in northern Iran and estimated PGA values of 0.3 g for 475- and 0.5 g to 0.75 g for 2475-year return periods. Grunthal [52] conducted a seismic-hazard assessment in Europe and estimated a PGA of 0.6 g for a 10% exceedance rate over 50 years. Zhang et al. [53] conducted a global seismic-hazard assessment in Asia. The highest expected PGA for a 10% exceedance rate over 50 years was estimated as 0.48 g in the Alpine–Himalayan belt. A comparative assessment of the PGA values observed in Eurasia in previous studies showed that the current results are good.

Spatially, the earthquake vulnerability can be understood from the resulting map developed for Eurasia. Approximately 60% of the population lives in very highly, highly, and moderately vulnerable zones. Notably, the high population and building density could be the reason behind the very-highly-to-highly vulnerable status of these areas in Eurasia. The rationale behind low vulnerability is minimal social characteristics. Thus, the developed vulnerability map can be considered as a source map for future risk mapping in Eurasia. For a detailed assessment, a country-scale vulnerability study is required, including various factors such as building types, the quality of materials and individual incomes, age groups, etc. Very-high- and high-earthquake risk areas should be considered by national governments for earthquake-mitigation planning. Moradi et al. [54] estimated earthquake vulnerability using the Choquet integral and the Shapley game theory. According to their results, highly dense populations and aged nonstandard buildings are very vulnerable to earthquakes. Ruggieri et al. [55] evaluated seismic vulnerability using a deep-convolutional-neural-network model for existing buildings by exploiting available photographs. Their results showed that the vulnerability index varied from 0.364 to 0.704 for different building classes, with an accuracy of 97%.

The earthquake risk (A and B) comparison was performed based on two risk-estimation formulas, which provide the basis for an accurate risk assessment (Figure 12). However, Risk A demonstrated that most parts of Japan, Indonesia, China, Afghanistan, Pakistan, India, Iran, Turkey, Tajikistan, and Kirgizstan were in very-high-risk areas, while according to Risk B, areas of very high risk were distributed in some specific locations in very highly earthquake-prone countries. In the case of the Risk A map, the risk was estimated using an industrial approach, through a multiplication of EPA and EVA (http://www.syque.com/quality_tools/tools/TOOLS11.htm, n.d. (accessed on 11 March 2022)) [56]. To generate Risk B, the product of EHA and EVA was calculated according to scientifically sound earthquake research [57]. The potential reasons behind the high level of risk include dense population, high building density, long active faults, high epicenter density, and high-magnitude events. The risk can be reduced in central Asia by considering the rehabilitation of the existing buildings, proper mitigation planning, and increasing the coping capacity [58]. Mangalathu et al. [59] conducted a regional earthquake-risk assessment for infrastructures using active machine learning. The results showed that the model achieved an accuracy of 80% for 100 bridge samples, which is equivalent to a model based on 480 bridge samples. Pelizari et al. [60] estimated earthquake risk using street-level imagery and a deep-convolutional-neural-network model. According to their results, the obtained output for the earthquake-prone Chilean capital, Santiago, showed an accuracy above $\kappa = 0.81$ in all the classification tasks. Hence, this study provides accurate results, and the proposed integrated AI method works efficiently.

The advantages and disadvantages of the integrated AI model depend on the execution, type of application, and data quality. Continent-scale earthquake-risk assessments using a robust integrated GRU–SRU model can provide accurate results. The SRU model was applied for the vulnerability estimation and was useful for prioritizing the criteria based on transfer-learning techniques.

This study provides evidence of accurate and comprehensive risk assessment on a continental scale. The limited studies on Himalayan collision zones and evidence of events show that the obtained results are accurate in terms of probability and risk [61–63]. However, the consolidation and inclusion of mitigation measures is necessary for the evaluation of the actual risk map using an appropriate risk-assessment strategy. The disadvantages of this study are associated with the integrated GRU–SRU model, which is data-dependent and needs large data set for an effective earthquake-probability study. The selection of appropriate criteria for probability mapping is necessary; otherwise, biased outputs may occur.

6. Conclusions

The objective of this research was to assess the earthquake risk in Eurasia on a continental. This is a new approach, and it was applied for the first time in Eurasia to estimate risk, followed by spatial probability, hazard, and vulnerability. The SPA was conducted at magnitudes above 5.5 Mw. Furthermore, in this study, an integrated deep transfer learning (GRU-SRU) model was implemented by considering several parameters based on the recent advances in DL models. In view of the geological and geo-structural distribution, as well as the level of urban development, very-high-risk areas were observed in central Eurasia, including Japan, Indonesia, China, India, Pakistan, Iran, Turkey, and some parts of Europe. The SPM showed that central Eurasia is at high risk due to its diverse and complex geo-tectonic environment. The hazard map showed that most of the hazard areas fall within the Alpine–Himalayan belt. These areas are characterized by a long history of earthquakes associated with high PGA and large events. Poor ground conditions may lead to high vulnerability. However, the renovation of old buildings and residential places is a primary task in central Asia and Europe, as well as eastern coastal countries in the Eurasian continent. The proposed integrated AI approach is a robust and efficient approach to future earthquake-risk estimation. The risk results indicated that (6,345,693 km^2) and (1,697,867 km^2) of the area is covered by a very-high-risk zone, based on Risk A and B, respectively. This Risk B map showed similar to the GEM-based risk map, which were acceptable, although the factors used were not the same. This work was limited to risk evaluation in the absence of liquefaction factors, fault characteristics, soil characteristics, and precursors. The criteria selection was based on a literature review for the site-specific and country-scale analysis; thus, it was transferable to a continent-scale study. The criteria were chosen strictly based on the historical catalog and geo-tectonic conditions. The aforementioned factors and randomly selected factors proved to be reliable for future probability and risk mapping, but they may not always be effective. Therefore, the current approach helps in reducing the computational complexity associated with risk assessment. In real-world scenarios, this study on earthquakes is crucial to formulate and implement state-of-the-art DL models. The traditional and previously developed models have uncertainties, including data dependency, accuracy, and modeling; addressing this detailed analysis will be a focus in the future.

Author Contributions: Conceptualization, R.J., A.S. and R.A.-R.; methodology, R.J., M.B.A.G., O.G., R.A.-R. and A.S.; software, R.J., A.S. and R.A.-R.; validation, R.J., A.S. and R.A.-R.; formal analysis, R.J., A.S., R.A.-R. and O.G.; investigation, R.J., A.S. and R.A.-R.; resources, R.J.; data curation, R.J.; writing—original draft preparation, R.J.; writing—review and editing, A.S., R.A.-R., B.P., M.B.A.G., O.G., H.M., M.A.K., P.G. and C.A.; visualization, R.J., A.S., R.A.-R., B.P. and O.G.; supervision, A.S. and R.A.-R.; project administration, R.A.-R. and A.S.; funding acquisition, A.S., R.A.-R., O.G. and C.A. All authors have read and agreed to the published version of the manuscript.

Funding: The work was funded by the GIS & Remote Sensing Center, Research Institute of Sciences and Engineering, University of Sharjah, UAE under the vice-chancellor research fund. The APC was funded by the Institute of Geomatics, University of Natural Resources and Life Sciences, Vienna, Austria.

Data Availability Statement: The data that support the findings of this study are available from the first author, (R.J.), upon reasonable request.

Conflicts of Interest: The authors declare no conflict of interest.

References

1. Aras, E.M.; Diaconeasa, M.A. A Critical Look at the Need for Performing Multi-Hazard Probabilistic Risk Assessment for Nuclear Power Plants. *Eng* **2021**, *2*, 454–467. [CrossRef]
2. Ahorner, L. *Protection of Nuclear Power Plants Against Seismic Effects Reference Ground Motion: Practice Followed in European Countries: (Synthesis Report)*; Harwood Academic for the Commission of the European Communities: London, UK, 1983.
3. Plichon, C.; Gueraud, R.; Richli, M.H.; Casagrande, J.F. Protection of Nuclear Power Plants against Seism. *Nucl. Technol.* **1980**, *49*, 295–306. [CrossRef]

4. Medel-Vera, C.; Ji, T. Seismic Protection Technology for Nuclear Power Plants: A Systematic Review. *J. Nucl. Sci. Technol.* **2015**, *52*, 607–632. [CrossRef]
5. Hakata, T. Seismic PSA Method for Multiple Nuclear Power Plants in a Site. *Reliab. Eng. Syst. Saf.* **2007**, *92*, 883–894. [CrossRef]
6. Damoom, M.M.; Hashim, S.; Aljohani, M.S.; Saleh, M.A.; Xoubi, N. Potential Areas for Nuclear Power Plants Siting in Saudi Arabia: GIS-Based Multi-Criteria Decision-Making Analysis. *Prog. Nucl. Energy* **2019**, *110*, 110–120. [CrossRef]
7. Pradhan, A.M.S.; Kim, Y.-T. An Artificial Intelligence-Based Approach to Predicting Seismic Hillslope Stability under Extreme Rainfall Events in the Vicinity of Wolsong Nuclear Power Plant, South Korea. *Bull. Eng. Geol. Environ.* **2021**, *80*, 3629–3646. [CrossRef]
8. Argyroudis, S.; Selva, J.; Gehl, P.; Pitilakis, K. Systemic Seismic Risk Assessment of Road Networks Considering Interactions with the Built Environment. *Comput. Civ. Infrastruct. Eng.* **2015**, *30*, 524–540. [CrossRef]
9. Pourghasemi, H.R.; Gayen, A.; Panahi, M.; Rezaie, F.; Blaschke, T. Multi-Hazard Probability Assessment and Mapping in Iran. *Sci. Total Environ.* **2019**, *692*, 556–571. [CrossRef]
10. Durlević, U.; Novković, I.; Lukić, T.; Valjarević, A.; Samardžić, I.; Krstić, F.; Batoćanin, N.; Mijatov, M.; Ćurić, V. Multihazard Susceptibility Assessment: A Case Study–Municipality of Štrpce (Southern Serbia). *Open Geosci.* **2021**, *13*, 1414–1431. [CrossRef]
11. Tang, Y.; Liu, S.; Li, X.; Fan, Y.; Deng, Y.; Liu, Y.; Yin, L. Earthquakes Spatio–Temporal Distribution and Fractal Analysis in the Eurasian Seismic Belt. *Rend. Lincei. Sci. Fis. Nat.* **2020**, *31*, 203–209. [CrossRef]
12. Zheng, W.; Li, X.; Yin, L.; Yin, Z.; Yang, B.; Liu, S.; Song, L.; Zhou, Y.; Li, Y. Wavelet Analysis of the Temporal-Spatial Distribution in the Eurasia Seismic Belt. *Int. J. Wavelets Multiresolut. Inf. Process.* **2017**, *15*, 1750018. [CrossRef]
13. Shebalin, P.; Zaliapin, I.; Keilis-Borok, V. Premonitory Raise of the Earthquakes' Correlation Range: Lesser Antilles. *Phys. Earth Planet. Inter.* **2000**, *122*, 241–249. [CrossRef]
14. Genmo, Z.; Zhonghai, W.; Jie, L.; Lei, Z.; Jiameng, Z. The Time Space Distribution Characteristics and Migration Law of Large Earthquakes in the Indiam-Eurasian Plate Collision Deformation Area. *J. Geomech.* **2019**, *25*, 324–340.
15. Ulomov, V.I. Structural and Dynamical Regularity of Eurasia Seismicity and Some Aspects of Seismic Hazard Prediction. *Proc. XXIV Gen. Ass. ESC* **1994**, *1*, 271–281.
16. Ulomov, V.I. Waves of Seismogeodynamic Activation and Long-Term Prediction of Earthquakes. *Fiz. Zemli* **1993**, *4*, 43–53.
17. Ulomov, V.I.; GSHAP Region 7 Working Group. Seismic hazard of northern Eurasia. *Ann. Geofis.* **1999**, *42*, 1023–1038. [CrossRef]
18. Rahman, M.M.; Bai, L.; Khan, N.G.; Li, G. Probabilistic Seismic Hazard Assessment for Himalayan–Tibetan Region from Historical and Instrumental Earthquake Catalogs. *Pure Appl. Geophys.* **2018**, *175*, 685–705. [CrossRef]
19. Bilham, R.; Gaur, V.K.; Molnar, P. Himalayan Seismic Hazard. *Science* **2001**, *293*, 1442–1444. [CrossRef]
20. Strakhov, V.N.; Ulomov, V.I.; Shumilina, L.S. New Maps of General Seismic Zoning of North Eurasia. *Izv. Phys. Solid Earth* **1998**, *34*, 872–876.
21. Lapajne, J. The MSK-78 Intensity Scale and Seismic Risk. *Eng. Geol.* **1984**, *20*, 105–112. [CrossRef]
22. Shapira, A. A Probabilistic Approach for Evaluating Earthquake Risks, with Application to the Afro-Eurasian Junction. *Tectonophysics* **1983**, *91*, 321–334. [CrossRef]
23. Gupta, G.D.; Srivastava, H.N. On Earthquake Risk Assessment in the Himalayan Region. *Mem. Geol. Soc. India* **1990**, *23*, 173–199.
24. Iakubovskii, D.; Komendantova, N.; Rovenskaya, E.; Krupenev, D.; Boyarkin, D. Impacts of Earthquakes on Energy Security in the Eurasian Economic Union: Resilience of the Electricity Transmission Networks in Russia, Kazakhstan, and Kyrgyzstan. *Geosciences* **2019**, *9*, 54. [CrossRef]
25. Jackson, J. Fatal Attraction: Living with Earthquakes, the Growth of Villages into Megacities, and Earthquake Vulnerability in the Modern World. *Philos. Trans. R. Soc. A Math. Phys. Eng. Sci.* **2006**, *364*, 1911–1925. [CrossRef]
26. Sarraz, A.; Ali, M.K.; Das, D.C. Seismic Vulnerability Assessment of Existing Building Stocks at Chandgaon in Chittagong City, Bangladesh. *Am. J. Civ. Eng.* **2015**, *3*, 1–8. [CrossRef]
27. Zanini, M.A.; Pellegrino, C.; Morbin, R.; Modena, C. Seismic Vulnerability of Bridges in Transport Networks Subjected to Environmental Deterioration. *Bull. Earthq. Eng.* **2013**, *11*, 561–579. [CrossRef]
28. Maio, R.; Ferreira, T.M.; Vicente, R.; Estêvão, J. Seismic Vulnerability Assessment of Historical Urban Centres: Case Study of the Old City Centre of Faro, Portugal. *J. Risk Res.* **2016**, *19*, 551–580. [CrossRef]
29. Asteris, P.G.; Chronopoulos, M.P.; Chrysostomou, C.Z.; Varum, H.; Plevris, V.; Kyriakides, N.; Silva, V. Seismic Vulnerability Assessment of Historical Masonry Structural Systems. *Eng. Struct.* **2014**, *62*, 118–134. [CrossRef]
30. Population of Europe (2019)—Worldometers. Available online: https://www.worldometers.info/world-population/europe-population/ (accessed on 24 July 2022).
31. Population of Asia (2019)—Worldometers. Available online: https://www.worldometers.info/world-population/asia-population/ (accessed on 24 July 2022).
32. Wani, A. India and China in Central Asia: Understanding the New Rivalry in the Heart of Eurasia. *Obs. Res. Found.* **2020**, *235*, 1–38.
33. Sarker, G.M. *Seismic Attenuation Variations at Range Fronts in Central Eurasia*; University of Kansas: Lawrence, KS, USA, 1998; ISBN 0599029633.
34. Ioffe, A.I. A Unified Seismotectonic Zonation of Northern Eurasia. *J. Earthq. Predict. Res.* **2000**, *8*, 8–31.
35. Batjes, N.H. *A Homogenized Soil Data File for Global Environmental Research: A Subset of FAO, ISRIC and NRCS Profiles (Version 1.0)*; ISRIC: Wageningen, The Netherlands, 1995.

36. Kong, Z.; Tang, B.; Deng, L.; Liu, W.; Han, Y. Condition Monitoring of Wind Turbines Based on Spatio-Temporal Fusion of SCADA Data by Convolutional Neural Networks and Gated Recurrent Units. *Renew. Energy* **2020**, *146*, 760–768. [CrossRef]
37. Wei, C.; Chen, L.; Song, Z.; Lou, X.; Li, D. EEG-Based Emotion Recognition Using Simple Recurrent Units Network and Ensemble Learning. *Biomed. Signal Process. Control* **2020**, *58*, 101756. [CrossRef]
38. Movsessian, A.; Cava, D.G.; Tcherniak, D. Interpretable Machine Learning in Damage Detection Using Shapley Additive Explanations. *ASCE-ASME J. Risk Uncertain. Eng. Syst. Part B Mech. Eng.* **2022**, *8*, 21101. [CrossRef]
39. Wang, Y.; Fang, Z.; Wang, M.; Peng, L.; Hong, H. Comparative Study of Landslide Susceptibility Mapping with Different Recurrent Neural Networks. *Comput. Geosci.* **2020**, *138*, 104445. [CrossRef]
40. Chung, J.; Gulcehre, C.; Cho, K.; Bengio, Y. Empirical Evaluation of Gated Recurrent Neural Networks on Sequence Modeling. *arXiv* **2014**, *preprint*. arXiv:1412.3555.
41. Lei, T.; Zhang, Y.; Wang, S.I.; Dai, H.; Artzi, Y. Simple Recurrent Units for Highly Parallelizable Recurrence. *arXiv* **2017**, *preprint*. arXiv:1709.02755.
42. Jiang, C.; Chen, S.; Chen, Y.; Bo, Y.; Han, L.; Guo, J.; Feng, Z.; Zhou, H. Performance Analysis of a Deep Simple Recurrent Unit Recurrent Neural Network (SRU-RNN) in MEMS Gyroscope de-Noising. *Sensors* **2018**, *18*, 4471. [CrossRef]
43. Bartier, P.M.; Keller, C.P. Multivariate Interpolation to Incorporate Thematic Surface Data Using Inverse Distance Weighting (IDW). *Comput. Geosci.* **1996**, *22*, 795–799. [CrossRef]
44. Xu, C.; Dai, F.; Xu, X.; Lee, Y.H. GIS-Based Support Vector Machine Modeling of Earthquake-Triggered Landslide Susceptibility in the Jianjiang River Watershed, China. *Geomorphology* **2012**, *145*, 70–78. [CrossRef]
45. Pan, S.J.; Yang, Q. A Survey on Transfer Learning. *IEEE Trans. Knowl. Data Eng.* **2010**, *22*, 1345–1359. [CrossRef]
46. Tan, C.; Sun, F.; Kong, T.; Zhang, W.; Yang, C.; Liu, C. A Survey on Deep Transfer Learning. In Proceedings of the 27th International Conference on Artificial Neural Networks (ICANN 2018), Rhodes, Greece, 4–7 October 2018; Springer: Berlin/Heidelberg, Germany, 2018; pp. 270–279.
47. Wang, H.; Wang, L.; Zhang, L. Transfer Learning Improves Landslide Susceptibility Assessment. *Gondwana Res.* **2022**. [CrossRef]
48. Aafaq, N.; Mian, A.; Liu, W.; Gilani, S.Z.; Shah, M. Video Description: A Survey of Methods, Datasets, and Evaluation Metrics. *ACM Comput. Surv.* **2019**, *52*, 1–37. [CrossRef]
49. Erdik, M.; Durukal, E. Earthquake Risk and Its Mitigation in Istanbul. *Nat. Hazards* **2008**, *44*, 181–197. [CrossRef]
50. Jena, R.; Pradhan, B.; Alamri, A.M. Susceptibility to Seismic Amplification and Earthquake Probability Estimation Using Recurrent Neural Network (RNN) Model in Odisha, India. *Appl. Sci.* **2020**, *10*, 5355. [CrossRef]
51. Abdollahzadeh, G.; Sazjini, M.; Shahaky, M.; Tajrishi, F.Z.; Khanmohammadi, L. Considering Potential Seismic Sources in Earthquake Hazard Assessment for Northern Iran. *J. Seismol.* **2014**, *18*, 357–369. [CrossRef]
52. Grunthal, G.; GSHAP Region 3 Working Group. Seismic Hazard Assessment for Central, North and Northwest Europe: GSHAP Region 3. *Ann. Geofis.* **1999**, *42*, 999–1011. [CrossRef]
53. Zhang, P.; Yang, Z.; Gupta, H.K.; Bhatia, S.C.; Shedlock, K.M. Global Seismic Hazard Assessment Program (GSHAP) in Continental Asia. *Ann. Geophys.* **1999**, *42*, 1167–1190. [CrossRef]
54. Moradi, M.; Delavar, M.R.; Moshiri, B. A GIS-Based Multi-Criteria Analysis Model for Earthquake Vulnerability Assessment Using Choquet Integral and Game Theory. *Nat. Hazards* **2017**, *87*, 1377–1398. [CrossRef]
55. Ruggieri, S.; Cardellicchio, A.; Leggieri, V.; Uva, G. Machine-Learning Based Vulnerability Analysis of Existing Buildings. *Autom. Constr.* **2021**, *132*, 103936. [CrossRef]
56. Aven, T. On Some Recent Definitions and Analysis Frameworks for Risk, Vulnerability, and Resilience. *Risk Anal. Int. J.* **2011**, *31*, 515–522. [CrossRef]
57. Kumpulainen, S. Vulnerability Concepts in Hazard and Risk Assessment. *Spec. Pap. Surv. Finl.* **2006**, *42*, 65.
58. Islam, R.; Islam, M.N.; Islam, M.N. Earthquake Risks in Bangladesh: Causes, Vulnerability, Preparedness and Strategies for Mitigation. *ARPN J. Earth Sci.* **2016**, *5*, 75–90.
59. Mangalathu, S.; Jeon, J.-S. Regional Seismic Risk Assessment of Infrastructure Systems through Machine Learning: Active Learning Approach. *J. Struct. Eng.* **2020**, *146*, 4020269. [CrossRef]
60. Pelizari, P.A.; Geiß, C.; Aguirre, P.; Santa María, H.; Peña, Y.M.; Taubenböck, H. Automated Building Characterization for Seismic Risk Assessment Using Street-Level Imagery and Deep Learning. *ISPRS J. Photogramm. Remote Sens.* **2021**, *180*, 370–386. [CrossRef]
61. Tiwari, A.; Paul, A.; Singh, R.; Upadhyay, R. Potential Seismogenic Asperities in the Garhwal–Kumaun Region, NW Himalaya: Seismotectonic Implications. *Nat. Hazards* **2021**, *107*, 73–95. [CrossRef]
62. Prasath, R.A.; Bansal, B.K.; Verma, M. Stress Distribution in the Western India-Eurasia Collision Zone, Its Kinematics and Seismotectonic Implications. *J. Asian Earth Sci.* **2022**, *230*, 105208. [CrossRef]
63. Negi, S.S.; Paul, A.; Cesca, S.; Kriegerowski, M.; Mahesh, P.; Gupta, S. Crustal Velocity Structure and Earthquake Processes of Garhwal-Kumaun Himalaya: Constraints from Regional Waveform Inversion and Array Beam Modeling. *Tectonophysics* **2017**, *712*, 45–63. [CrossRef]